N91-21196

FIVE DEGREE-of-FREEDOM CONTROL of an ULTRA-PRECISION MAGNETICALLY-SUSPENDED LINEAR BEARING

David L. Trumper

University of North Carolina at Charlotte

Department of Electrical Engineering

Charlotte

NC 28223

A.H. Slocum

Cranfield Institute of Technology

Cranfield Institute for Precision Engineering

Cranfield

Bedford MK43 0AL

England

Five-Degree-of-Freedom Control of an Ultra-Precision Magnetically-Suspended Linear Bearing.

David L. Trumper
Dept. of Electrical Engineering
Univ. of N. Carolina at Charlotte
Charlotte, NC 28223

Alexander H. Slocum
Cranfield Unit for Prec. Eng.
Cranfield Inst. of Tech.
Cranfield, Bedford MK43 OAL
England

1 Introduction

Highly-precise positioning is important in many aerospace applications. Magnetic bearings represent an attractive approach for achieving this positioning. The authors have constructed a high precision linear bearing which represents the experimental implementation of an idea presented in [1]. This system has been investigated as part of the the first author's Ph.D. thesis [2].

A 10.7 kg platen measuring 125 mm by 125 mm by 350 mm is suspended and controlled in five degrees of freedom by seven electromagnets. Position of the platen is measured by five capacitive probes which have nanometer resolution. The suspension acts as a linear bearing, allowing linear travel of 50 mm in the sixth degree of freedom. In the laboratory this bearing system has demonstrated position stability of 5 nm peak-to-peak. This is believed to be the highest position stability yet demonstrated in a magnetic suspension system. Performance at this level confirms that magnetic suspensions can address motion control requirements at the nanometer level.

The experimental effort associated with this linear bearing system is described. Major topics are the development of models for the suspension, implementation of control algorithms, and measurement of the actual bearing performance. Suggestions for future improvement of the bearing system are given.

2 System Overview

The linear bearing system grew out of the Ångstrom Resolution Measuring Machine (ÅRMM) proposed in [1]. The operating principle of the ÅRMM is to suspend a platen using seven electromagnets such that the platen is capable of 50 mm travel in the direction of the long axis of the platen. Two such suspended platens are then arranged so that their long axes of travel are perpendicular and lie in a horizontal plane. In this manner a sample attached to one platen can be scanned by a probe attached to the second platen. Thus the sample can be scanned over a square area of length and width equal to the travel of the two platens.

In the current work, a single platen-suspension was built in order to demonstrate proof-of-concept for this system. The basic operating principles of the linear bearing suspension are described in the remainder of this section.

Three electromagnets act on the top surface of the platen and four electromagnets act on the sides of the platen. The three top electromagnets serve to control the platen's roll, pitch and vertical translation. Gravity is used to bias the suspension so as to supply force in the downward direction. The four side electromagnets are arranged in pairwise opposition, two on each side of the platen, so as to act in a push-pull fashion. These electromagnets control the platen's yaw and lateral translation. The sixth degree of freedom which is translation in the direction of the long axis of the platen is currently not controlled.

Since five platen degrees of freedom are controlled, five independent position measurements are required. This is achieved by locating capacitance probes in the center of each of the three top electromagnets and in the center of two side magnets. This arrangement allows the measurement of the five controlled platen degrees of freedom. Travel in the long axis of the platen is not measured in our implementation.

The platen consists of a hollow, rectangular-section steel tube, with dimensions of 125 mm by 125 mm by 350 mm. This tubular form was chosen to be compatible with the taut-wire inchworm driver

proposed in [1] to effect travel in the long axis of the platen. This inchworm drive was not implemented in the current effort.

The manner in which the electromagnet forces act on the platen is shown in Figure 1. Here, each arrow represents the force applied by the corresponding electromagnet. This force is normal to the platen, and acts through the center of the electromagnet. The black dots in the figure indicate the locations at which the capacitance probes measure position.

A mechanical drawing of the platen is shown in Figure 2. It consists of a 5 inch square steel tube which was surface ground on all four faces for mechanical accuracy, nickel plated to prevent corrosion, and then annealed for better magnetic properties and dimensional stability. The platen weighs 10.7 kilograms.

The design uses one large electromagnet and six small electromagnets. Both types contain a permanent magnet as well as the electromagnet coil. The electromagnets are glued into aluminum blocks, which are then bolted to cast-iron support brackets on both sides of the platen. When not in suspension, the platen rests on a three-legged table referred to as the landing pad. The assembled system is shown in the mechanical drawings of Figures 3, 4, and 5. The 0.005" air gap between the platen and the bearing faces is too small to be seen in these views.

3 Linear Model

A linear model for the suspension dynamics is developed by first achieving active suspension through empirical tuning of the suspension controller as described in [2]. Once suspension is achieved, the magnet force linear parameters are measured through the experiment described in the next section. These linear parameters are then inserted into a linear dynamical model to yield the suspension linear model. This model is valid for small motions about the nominal operating point where the platen is centered between the electromagnets and centered in the axial degree of freedom.

3.1 Magnet Force Experiments

The force/position/current characteristics of the three top electromagnets are measured as follows. The platen is suspended at the nominal operating point (zero volts on each position probe), and the seven current drive bias potentiometers are adjusted so that the five modal control signals are approximately zero. That is, in this state, the DC component of current in each drive is supplied by the bias potentiometer setting. An additional mass is placed inside the platen, resting on the center of the bottom face of the interior of the platen. In this manner, the additional mass is directly below the platen center of mass. Thus, an additional force of Mg is applied to the platen, with no resulting torques about the platen center of mass. Four masses are used: 50, 100, 200, and 500 grams, respectively. For each mass value, the platen is cycled through a range of approximately $\pm 17\mu$m in vertical translation. At 20 points in this range, the three top magnet coil currents and the three top probe voltages are measured. The resulting data for the large top magnet shown in Figure 6. The data for the two small top electromagnets are similar and are not shown here.

The electromagnet force data is fitted in the least squares sense to the linearized force model

$$i = mx + cF + d, \tag{1}$$

or

$$F = \frac{1}{c}i - \frac{m}{c}x - \frac{d}{c}, \tag{2}$$

where F is the additional force applied to the magnet, i is the coil current, x is the probe voltage, and m, c, and d are constants to be determined by the least squares fit. Note that d represents the operating point bias current.

A small hysteresis effect is present in the magnet force curves. This results from hysteresis in the electromagnet and platen materials. Also, the curves do not form closed loops; this is due to the fact that the set of measurements for each loop required approximately 30 minutes to complete. For the development of the linearized model, the hysteresis is absorbed by the averaging process, as all data

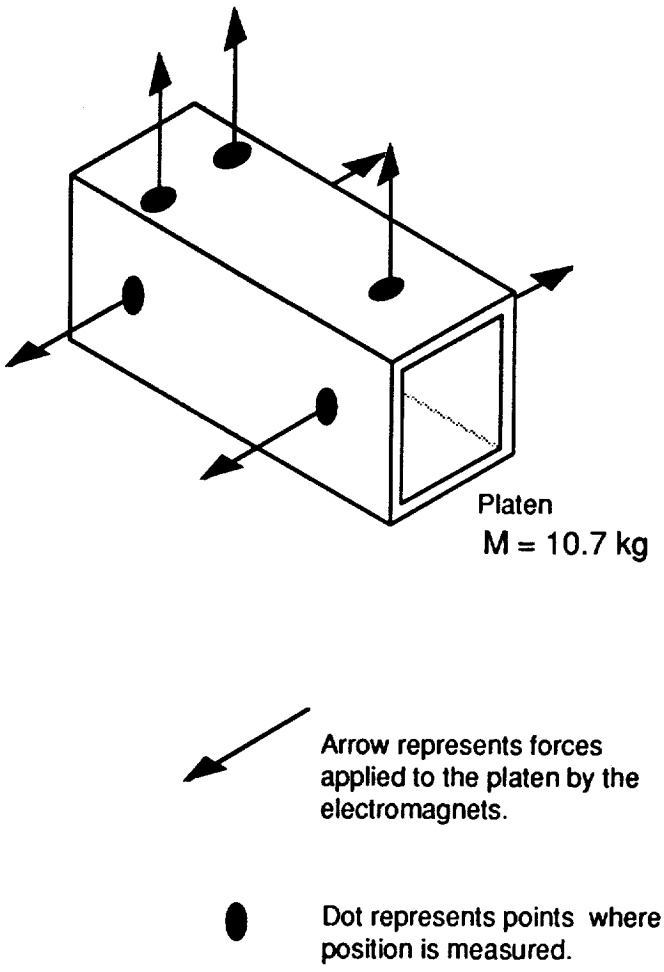

Figure 1: Schematic view of platen showing application of electromagnet forces and location of capacitance-probe position measurements.

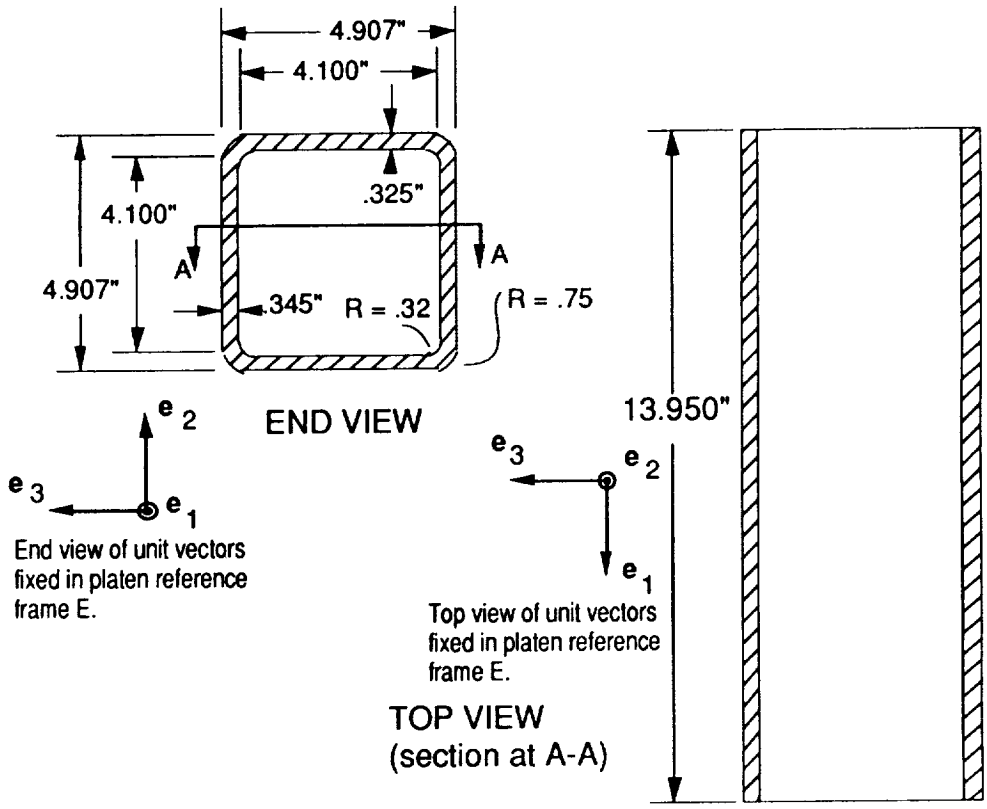

Figure 2: Platen mechanical drawings. Body frame E coordinates are shown.

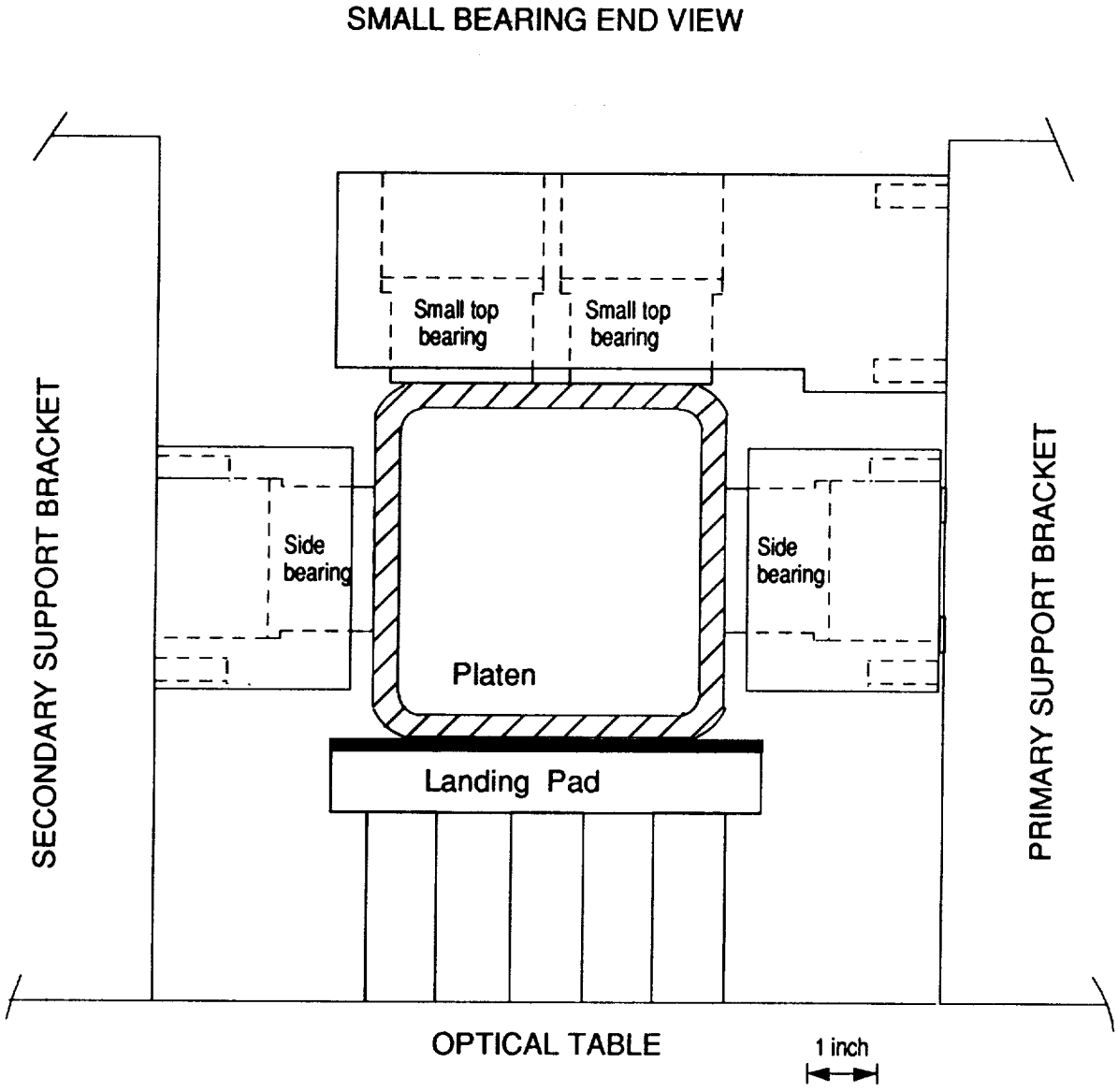

Figure 3: Suspension system small bearing end view.

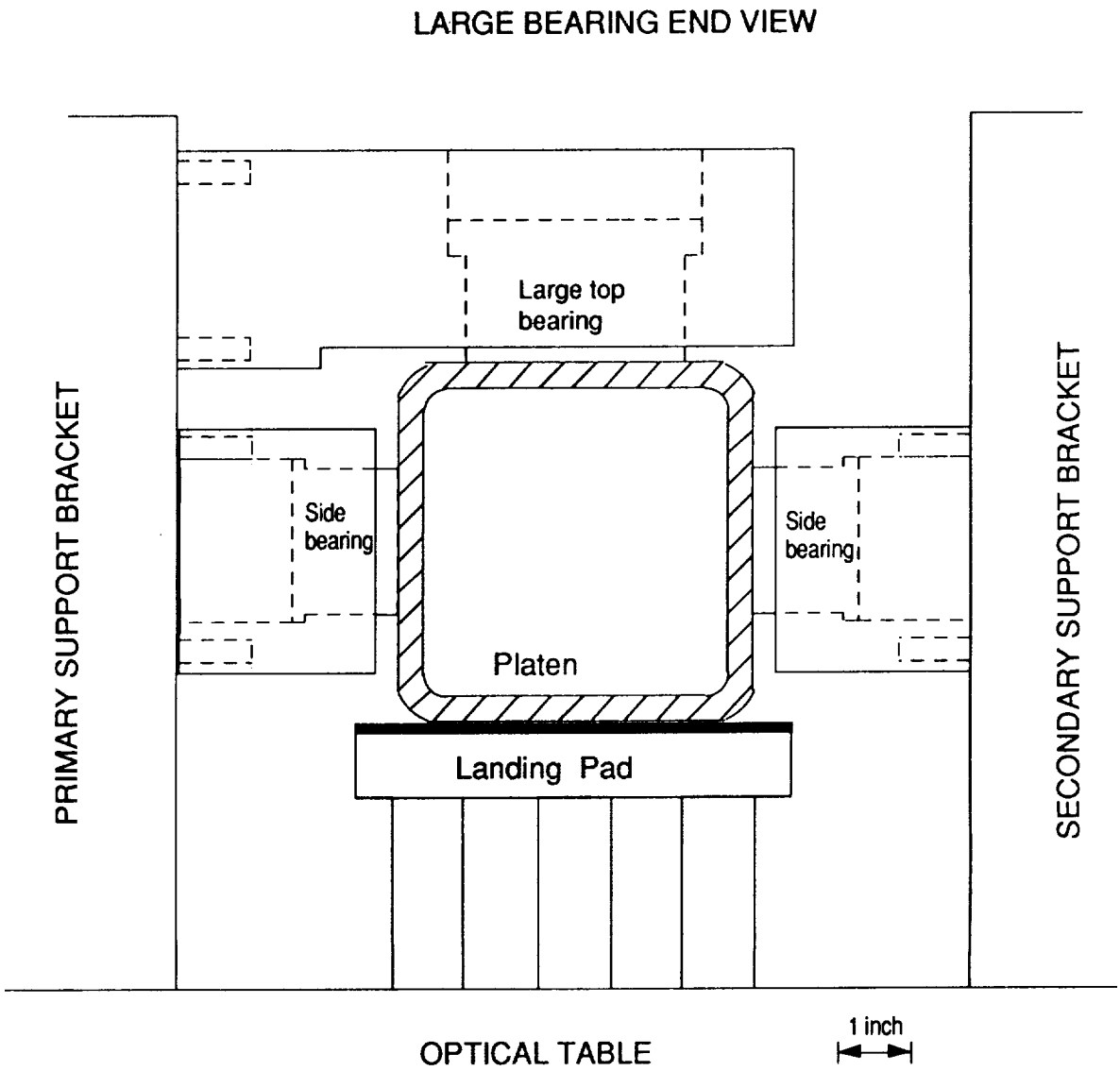

Figure 4: Suspension system large bearing end view.

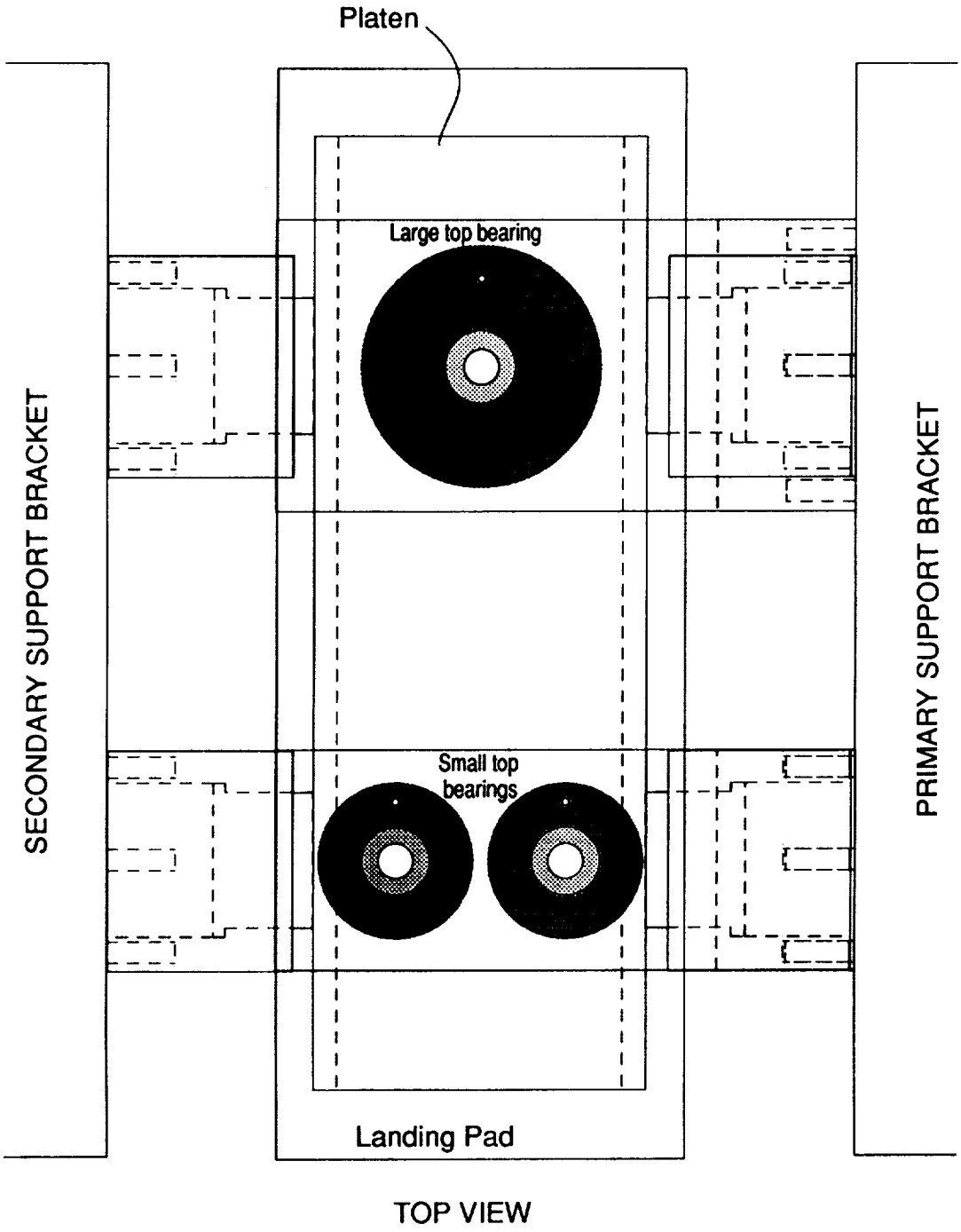

Figure 5: Suspension system top view.

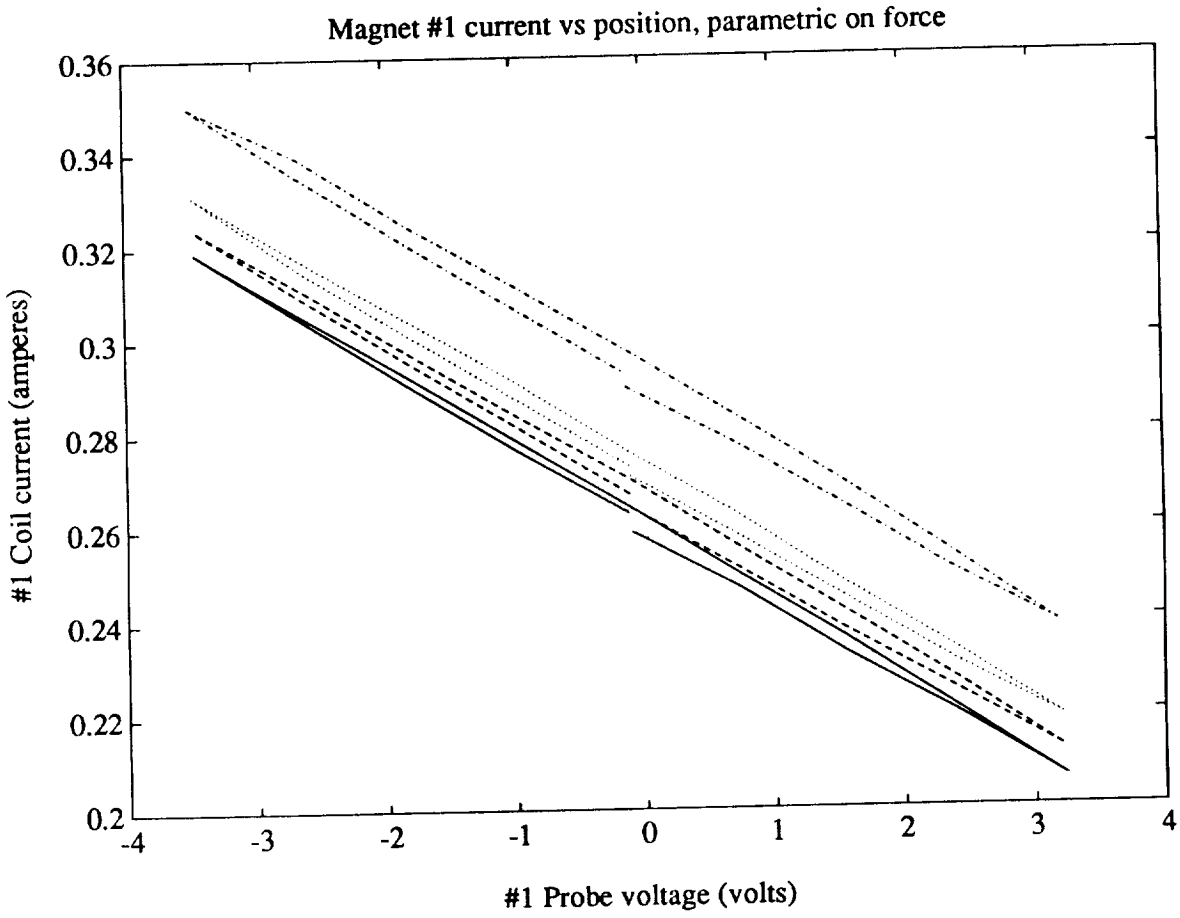

Figure 6: Magnet #1 (large) coil current vs. position probe voltage, for four additional mass values: 50, 100, 200, and 500 grams respectively from bottom to top.

points are given equal weight in the least squares fit. This is equivalent to taking the centerline of the hysteresis curve.

Two models are developed, one for the large magnet and one for the small magnets. The two top magnets are assumed to be identical, and their characteristics are averaged before fitting parameters. Note that the large magnet carries half the additional load, and each of the small magnets carry one fourth of the additional load. For the large magnet, the least squares fit is given by the parameters $m = -1.68 \times 10^{-2}$ amps/volt, $c = 1.36 \times 10^{-4}$ amps/gram, and $d = 2.58 \times 10^{-1}$ amps. For the small magnet, the least squares fit is given by the parameters $m = -1.94 \times 10^{-2}$ amps/volt, $c = 2.81 \times 10^{-4}$ amps/gram, and $d = 5.04 \times 10^{-1}$ amps.

For the purposes of control, the magnet linear force models are represented by $\tilde{F}_j = k_i \tilde{i}_j + k_x \tilde{x}_j$ where $\tilde{F}_j$, $\tilde{i}_j$, and $\tilde{x}_j$ are the j^{th} electromagnet incremental force, current, and air-gap, respectively. The constants k_i and k_x are determined from the force measurements. For the large magnet this yields $k_{il} = 7.21 \times 10^1$ Newtons/amp, and $k_{xl} = 2.38 \times 10^5$ Newtons/meter. For the small electromagnet, $k_{is} = 3.49 \times 10^1$ Newtons/amp, and $k_{xs} = 1.33 \times 10^5$ Newtons/meter. Here, the subscripts l and s are appended to indicate the large and small electromagnets respectively.

Experiments similar to those described above were also conducted to measure the magnet torques exerted on the platen [2]. These torque terms were then included in the dynamic model.

Since the four lateral magnets are operated at approximately the same bias currents and air gaps as the two small top magnets, the parameters developed here apply to the lateral magnets as well.

A dynamic analyzer was used to measure the suspension transfer functions. The measured transfer functions had a higher roll-off rate at high frequencies than would be predicted by just Newton's law, i.e., greater than $1/\omega^2$. It was found to be necessary to add a pair of poles to the model to match this roll-off. These poles have time constants of 0.6 and 0.2 msec respectively and are included in series with each coil current.

The platen mass is 10.7 kg. Its moments of inertia are calculated as $I_1 = 4.76 \times 10^{-2}$ kg m^2, $I_2 = 1.37 \times 10^{-1}$ kg m^2, and $I_3 = 1.35 \times 10^{-1}$ kg m^2 about the $\mathbf{e}_1$, $\mathbf{e}_2$, and $\mathbf{e}_3$ axes respectively. All suspension magnets are axially displaced from the platen center of mass by a distance $L_m = 92.1$mm. The two top electromagnets are also laterally displaced by a distance $W_m = 31.8$mm.

Using this information and the magnet force models developed above yields the suspension state equations. The vertical and lateral dynamics are essentially uncoupled. That is, vertical translation, roll and pitch motions which are controlled by the three top electromagnets, are essentially decoupled from lateral translation and yaw motions which are controlled by the four side magnets. The control design issues for the two decoupled systems are thus considered independently. In the remainder of this report we focus on the vertical system. For similar issues addressed in the control of the lateral system see [2].

The suspension state equations for the vertical dynamics are

$$\dot{w}_v = A_v w_v + B_v i_v \tag{3}$$

$$y_v = C_v w_v \tag{4}$$

where $w_v = [\, w_{v1}\ w_{v2}\ w_{v3}\ w_{v4}\ w_{v5}\ w_{v6}\ \tilde{q}_1\ \tilde{q}_3\ \tilde{x}_2\ \tilde{u}_1\ \tilde{u}_3\ \tilde{u}_5\,]'$, $i_v = [\, \tilde{i}_1\ \tilde{i}_2\ \tilde{i}_3\,]'$, and $y_v = [\, \tilde{q}_1\ \tilde{q}_3\ \tilde{x}_2\,]'$. Here, $w_{v1} \cdots w_{v6}$ are states associated with the high-frequency poles, $\tilde{q}_1$ is incremental rotation in radians about the $\mathbf{e}_1$ axis, $\tilde{q}_3$ is incremental rotation in radians about the $\mathbf{e}_3$ axis, and $\tilde{x}_2$ is incremental translation in meters in the $\mathbf{e}_2$ axis. State variables $\tilde{u}_1$, $\tilde{u}_3$, and $\tilde{u}_5$ are rotational and linear velocities given by the time derivatives of $\tilde{q}_1$, $\tilde{q}_3$, and $\tilde{x}_2$, respectively. Currents i_1, i_2, and i_3 are the coil currents in the single large and two small top electromagnets, respectively. The numerical values of the system matrices A_v, B_v, C_v, and D_v are given in the Appendix.

4 Controller Design

The controller design is based upon the linear suspension state equations given in the previous section. The controller is designed to decouple modal motions about the principal axes of the platen and is implemented in analog electronics. Only the vertical system controller is presented here.

The modal controller design includes a network at the input of the plant which serves to convert from modal control signals to individual current setpoints and a network at the output of the plant which

converts from the individual probe voltages to signals which represent the modal motions. A block diagram showing this control architecture is given in Figure 7. All the data paths carry three-vectors, although they are shown as single lines in the figure.

The open-loop suspension dynamics, current-drive dynamics and controller dynamics are given by their associated system matrices. The matrix T_{py} transforms the platen position y into the probe voltages v_p. The matrix T_{mp} transforms the the probe voltages v_p into voltages v_m which represent motions in the roll, pitch and vertical translation modes. The voltages v_m are subtracted from the modal setpoints v_s to give the modal errors v_e. These three errors are processed by three independent modal controllers to give the control voltages v_u which represent drives to the three modes. The matrix T_{iu} transforms the control voltages v_u into voltages v_i which control the current setpoints for the three current drives. The current drives establish currents i which act as inputs to the plant, thereby driving the platen position y.

The position probes have a sensitivity of 5 volts per 0.001" or 1.97×10^5 volts per meter, increasing as the air gap decreases. Thus the matrix T_{py} is given by

$$T_{py} = 1.97 \times 10^5 T_{gy} = \begin{bmatrix} 0 & -1.81 \times 10^4 & 1.97 \times 10^5 \\ 6.25 \times 10^3 & 1.81 \times 10^4 & 1.97 \times 10^5 \\ -6.25 \times 10^3 & 1.81 \times 10^4 & 1.97 \times 10^5 \end{bmatrix} \tag{5}$$

where T_{gy} transforms from the suspension position to the three probe air-gaps, and is given by

$$T_{gy} = \begin{bmatrix} 0 & -L_m & 1 \\ W_m & L_m & 1 \\ -W_m & L_m & 1 \end{bmatrix} = \begin{bmatrix} 0 & -0.0921 & 1 \\ 0.0318 & 0.0921 & 1 \\ -0.0318 & 0.0921 & 1 \end{bmatrix} \tag{6}$$

The matrix T_{mp} is defined as

$$T_{mp} = \begin{bmatrix} 0 & 0.5 & -0.5 \\ -0.5 & 0.25 & 0.25 \\ 0.5 & 0.25 & 0.25 \end{bmatrix} \tag{7}$$

The relative scaling of the elements in the array is dictated by the suspension geometry. The absolute levels are chosen so that the voltages v_m saturate[1] only when all three probe outputs are saturated. The transformation T_{mp} is implemented in op-amp circuitry as shown in Figure 8.

The matrix T_{iu} is defined as

$$T_{iu} = \begin{bmatrix} 0 & -1 & 1 \\ 1 & 1 & 1 \\ -1 & 1 & 1 \end{bmatrix} \tag{8}$$

The relative scaling of the elements in the array is dictated the ratio of the large and small magnet current constants. That is, the magnitude ratio of the 1-2 and 1-3 entries to the 2-2, 3-2, 2-3, and 3-3 entries is equal to $2 * k_{is}/k_{il}$ which is approximately equal to unity. The absolute levels are chosen so that the entries are of unity magnitude. This allows an easier circuit implementation and is such that a single modal control signal can saturate the current drives. The transformation T_{iu} is implemented in op-amp circuitry as shown in Figure 9.

4.1 Current drive implementation

The current drive circuit implementation is shown in Figure 10. Current is sensed with a 1 Ω power resistor, and controlled via the IRF510 power FET. The coil is protected with a 2 amp fuse, and the series combination of the MUR1560 diode and 5 Ω resistor form a flyback network to allow coil current to continue to flow even when the FET is turned off suddenly. The 0.01 μF capacitor connected between the FET drain and ground is empirically selected to damp a closed-loop oscillation at about 500 kHz. A shown in the schematic, the +12 return, analog ground, and chassis ground are connected at only one point, in order to ensure that no coil currents flow in the analog ground; the common point is at the ground end of the current sense resistor. In parallel with the 1 Ω current sense resistor, a 50 μA meter in series with a 37.5 kΩ resistor provides a front-panel indication of coil current.

[1] The probe outputs and the op amps used to implement these coordinate transformations saturate at about ±13 volts.

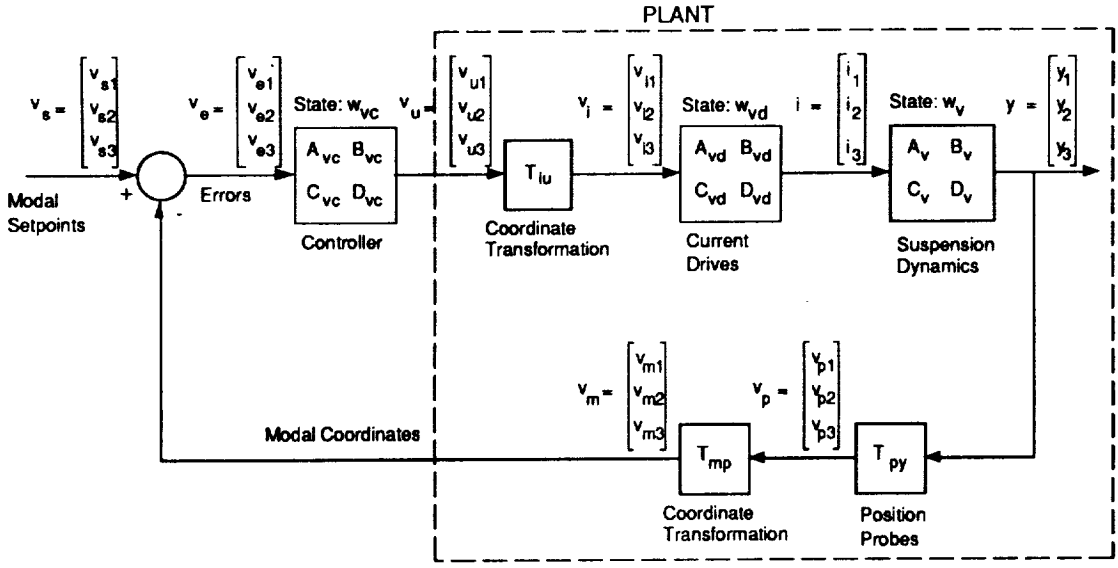

Figure 7: Block diagram for the vertical control loop.

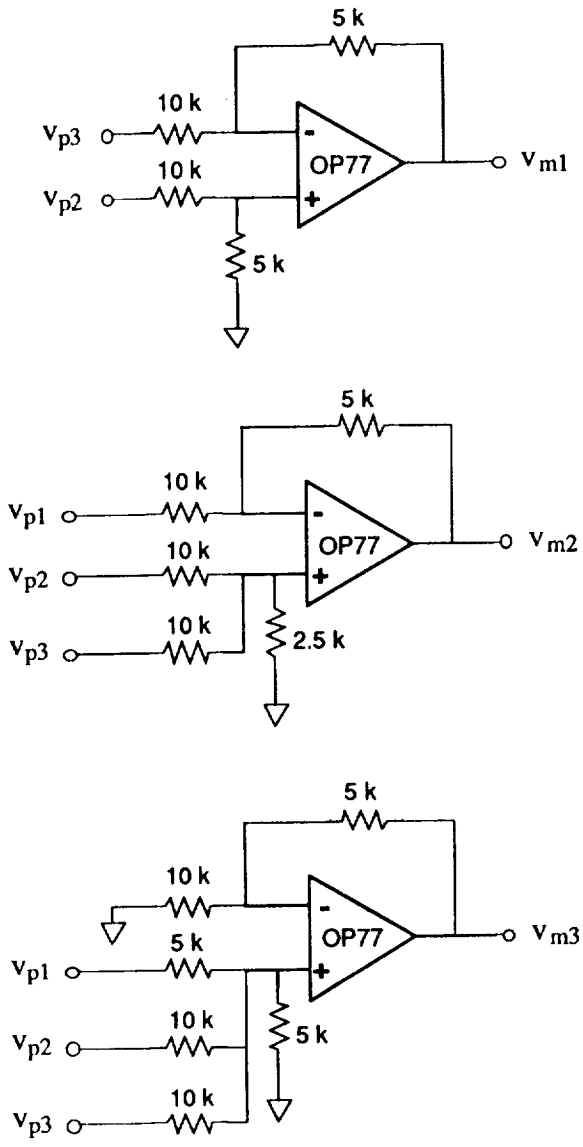

Figure 8: Circuit implementation of the transformation T_{mp}.

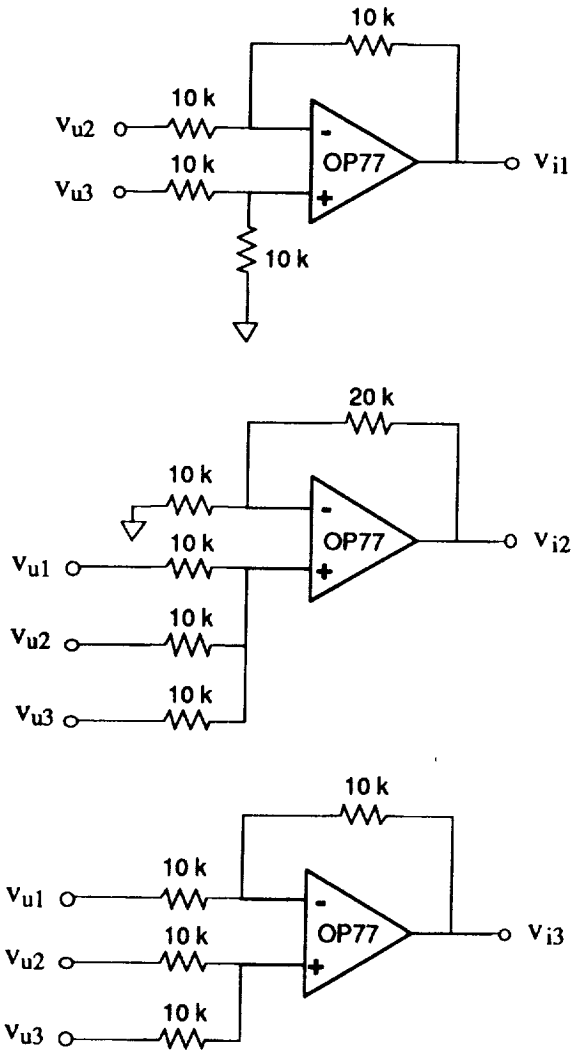

Figure 9: Circuit implementation of the transformation T_{iu}.

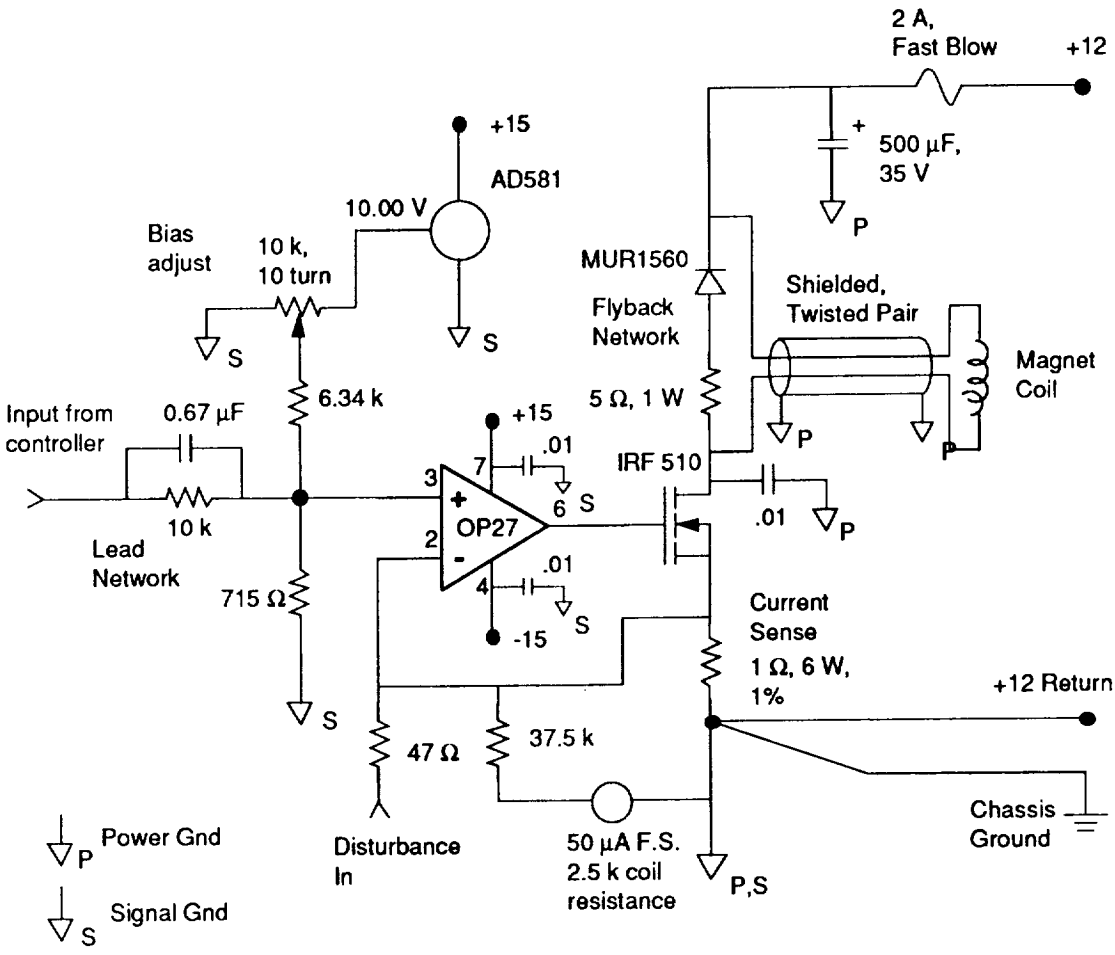

Figure 10: Current source for driving electromagnets.

The OP-27 op amp is used as the current controller for its low noise (especially in the 0.1–10 Hz band), high slew rate, and wide frequency response. The network at the noninverting input allows setting the DC current level through a 10 kΩ, 10 turn potentiometer, and couples current input signals through a lead network with a DC attenuation of 15, and unity gain at high frequencies. This lead network is included here because all anticipated position controller designs require lead compensation in the vicinity of crossover, and this allowed saving an additional stage in the position controller circuitry. Such savings are important, as five position control channels need to be constructed.

With the input attenuation of 15 and the 1 Ω current sense resistor, the amplifier has a closed-loop response of 15 Volts input per ampere of coil current output. The 47 Ω resistor at the inverting input of the OP-27 allows the injection of disturbances into the current loop and is of the correct resistance to be driven by a standard signal generator. An AD581 voltage reference supplies 10 Volts to bias the upper end of the potentiometer.

The large magnet has a coil resistance $R_{cl} = 4.4\ \Omega$, and inductance $L_{cl} = 48$ mH at the nominal operating point. The small magnet has a coil resistance $R_{cs} = 2.9\ \Omega$, and inductance $L_{cs} = 19$ mH at the nominal operating point.

Including the lead compensation term, each of the current drives has a transfer function from input v_{ij} to output i_j given by

$$\frac{i_j(s)}{v_{ij}(s)} = \frac{1}{\alpha}\frac{\alpha\tau s + 1}{\tau s + 1} \tag{9}$$

where $\alpha = 15$ and $\tau = 4.47 \times 10^{-4}$. Combining the three vertical system current drives in parallel yields the current source system equations as

$$\dot{w}_{vd} = A_{vd}w_{vd} + B_{vd}v_i \tag{10}$$
$$i = C_{vd}w_{vd} + D_{vd}v_i \tag{11}$$

where

$$A_{vd} = \mathrm{diag}(-2.24 \times 10^3,\ -2.24 \times 10^3,\ -2.24 \times 10^3) \tag{12}$$
$$B_{vd} = \mathrm{diag}(1,\ 1,\ 1) \tag{13}$$
$$C_{vd} = \mathrm{diag}(-2.09 \times 10^3,\ -2.09 \times 10^3,\ -2.09 \times 10^3) \tag{14}$$
$$D_{vd} = \mathrm{diag}(1,\ 1,\ 1) \tag{15}$$

For the purposes of design, the region contained within the dashed line in Figure 7 is considered to be the plant which is controlled by the controller. Combining all the information developed above yields the plant system matrices as

$$\dot{w}_{vp} = A_{vp}w_{vp} + B_{vp}v_u \tag{16}$$
$$v_m = C_{vp}w_{vp} + D_{vp}v_u \tag{17}$$

where $w_{vp} = [\ w_v'\ \ w_{vd}'\ ]'$ and

$$A_{vp} = \begin{bmatrix} A_v & B_vC_{vd} \\ 0 & A_{vd} \end{bmatrix} \tag{18}$$

$$B_{vp} = \begin{bmatrix} B_vD_{vd}T_{iu} \\ B_{vd}T_{iu} \end{bmatrix} \tag{19}$$

$$C_{vp} = [\ T_{mp}T_{py}C_v \quad 0\ ] \tag{20}$$

$$D_{vp} = [0] \tag{21}$$

where the indicated zero blocks are of the appropriate dimensions.

The three vertical system controllers take the form of lag-compensators. Lag compensation is used to develop higher disturbance rejection. Recall that the current drives already implement lead compensation; the lead term is necessary in order to stabilize the loops. The controllers use lag networks with a lag factor of only ten. This does not allow as good disturbance rejection as controllers which place the lag pole at the origin by using an integrator. However it is very difficult to initialize the suspension if

integrators are used in the compensator. This difficulty is due to integrator windup. In the future, the best solution is to use a dual-mode controller which gates-out an integral term until the suspension is initialized.

The controllers are designed under the assumption that the plant is decoupled. That is, the roll controller is designed to control the transfer function $v_{m1}(s)/v_{u1}(s)$, the pitch controller is designed to control the transfer function $v_{m2}(s)/v_{u2}(s)$, and the heave controller is designed to control the transfer function $v_{m3}(s)/v_{u3}(s)$. All three controllers take the form of lag compensators designed for a 100 Hz crossover.

The controller designs are

$$\frac{v_{ui}(s)}{v_{ei}(s)} = k_i \frac{\tau_a s + 1}{\tau_b s + 1} \qquad i = 1,2,3 \tag{22}$$

where τ_a = 9.1 milliseconds, τ_b = 100 milliseconds, k_1 = 111, k_2 = 17, and k_3 = 12. The circuit implementation of the transfer functions (22) is shown in Figure 11.

The only difference among the three controllers is in the value of the DC gain which is set by the resistor R_i'. The roll controller has R_1' = 1 k, the pitch controller has R_2' = 6.5 k, and the heave controller has R_3' = 9.6 k, as shown in the figure.

The compensation of the three loops is similar and thus only the roll loop will be presented. The loop-transmission in roll is shown in Figure 12 and the predicted step-response in roll is shown in Figure 13. The measured roll step response shown in Figure 14 matches the predicted response very closely. Specifically, the time from the beginning of the step to the first peak is about 5 msec in both the predicted and measured responses, and the peak-overshoot value is about 1.75 times the final value. The step response was averaged on a digital oscilloscope to reduce the noise background.

The large overshoot in the step response is due primarily to the inclusion of the lead compensation in the loop forward path. This overshoot could be reduced by preceding the loop with a command pre-filter, or more simply, by including the lead compensation in the feedback path. Since the lead network has a DC gain of unity, this option would not compromise low-frequency position accuracy.

The second trace in Figure 14 shows the cross-coupling into the platen pitch motion. The pitch response is not symmetric with respect to the two step edges; this indicates that even at these small signal-levels, nonlinear terms are significant.

Note that when the step in roll occurs, the initial cross-coupling transient is toward positive pitch in both cases. This observation can be explained by the nonlinearity in electromagnet force as a function of current. At the edge of the step-command in roll, the currents in the two small top electromagnets are driven differentially away from their operating point values. For steps where the air-gaps change by as little as 50 nm, the initial current transients have magnitudes of several tenths of an Ampere.

This is a large variation relative to the operating point current of 0.5 Ampere. Since the electromagnet force varies as i^2, symmetrically increasing and decreasing the small top electromagnet currents will result in a net *increase* in the sum of the two electromagnet forces. This increase is independent of the direction of the roll step. Increased force from the small electromagnets drives the platen in the positive pitch direction. Thus the initial transient will be in the direction of increasing pitch independent of the direction of the step in roll.

As before, including a command prefilter, or placing the lead compensation in the feedback path will greatly reduce the magnitude of the transient currents and thereby the magnitude of the nonlinear cross-coupling. This effect can also be overcome even for large steps by including nonlinear compensation laws in the controller which invert the electromagnet nonlinearity [3].

5 Position Stability

The closed-loop system has demonstrated 5 nm position stability. However, due to a flaw in the electronics of the position probes, this stability can be demonstrated only in three degrees of freedom. If more than three of the capacitance probes are used simultaneously, a very significant cross-talk between the channels results.

The five position probes operate by sensing a capacitance which varies with the spacing between the probe and platen. The five probes are inserted and glued into the central hole in the three top electromagnets and in the two primary side electromagnets. By this arrangement, motion can be measured in

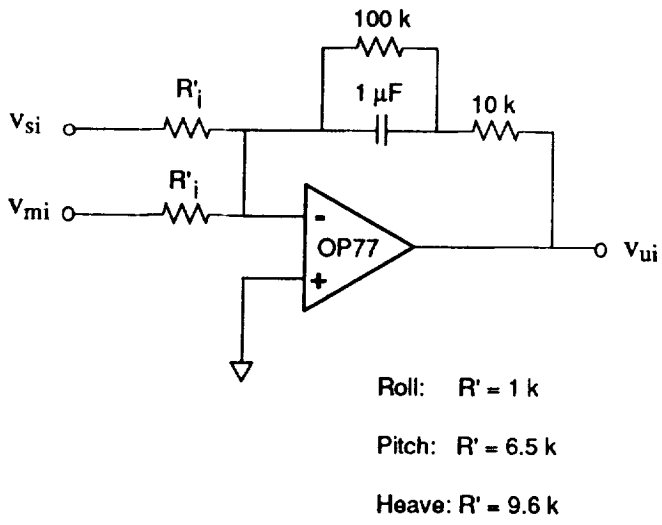

Figure 11: Vertical controller circuit implementation.

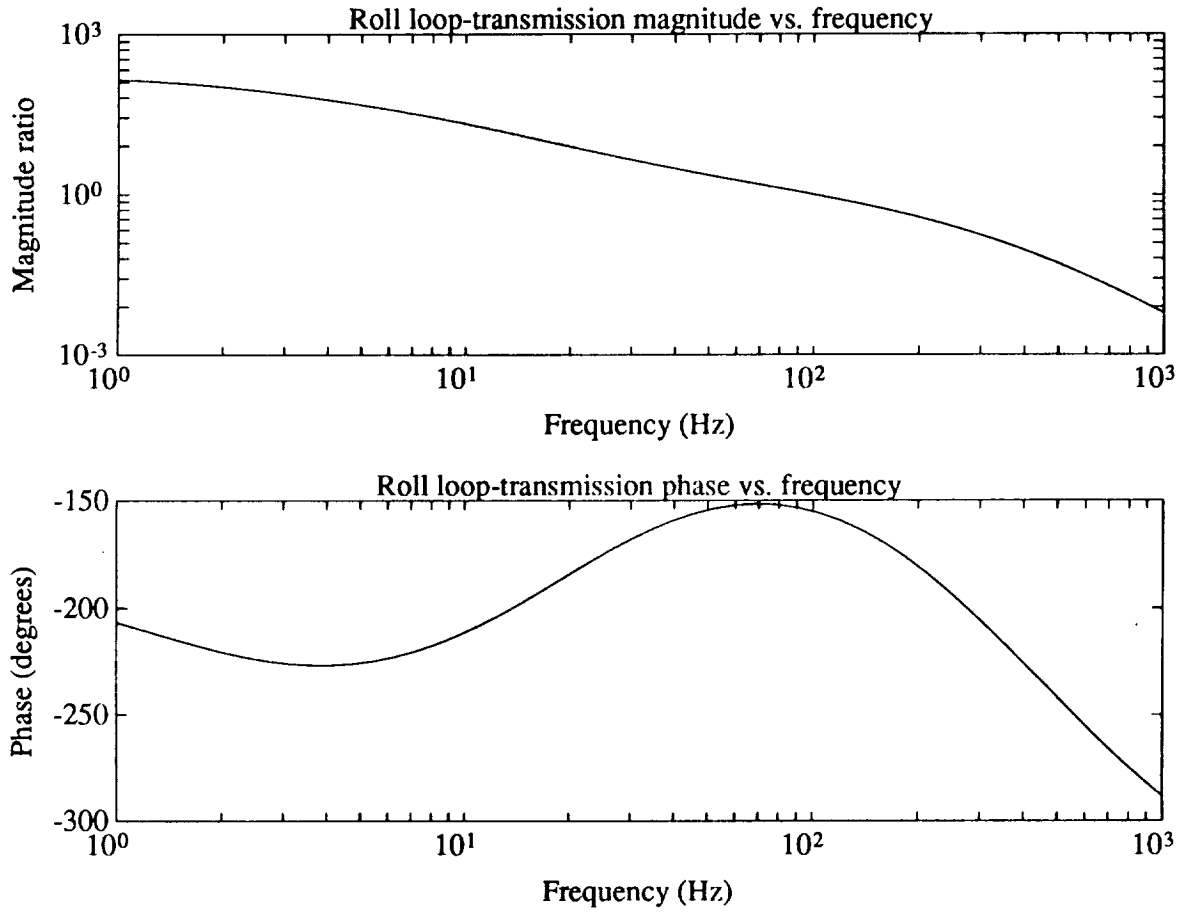

Figure 12: Roll loop-transmission $v_{m1}(s)/v_{e1}(s)$ magnitude and phase versus frequency. Crossover is at 100 Hz.

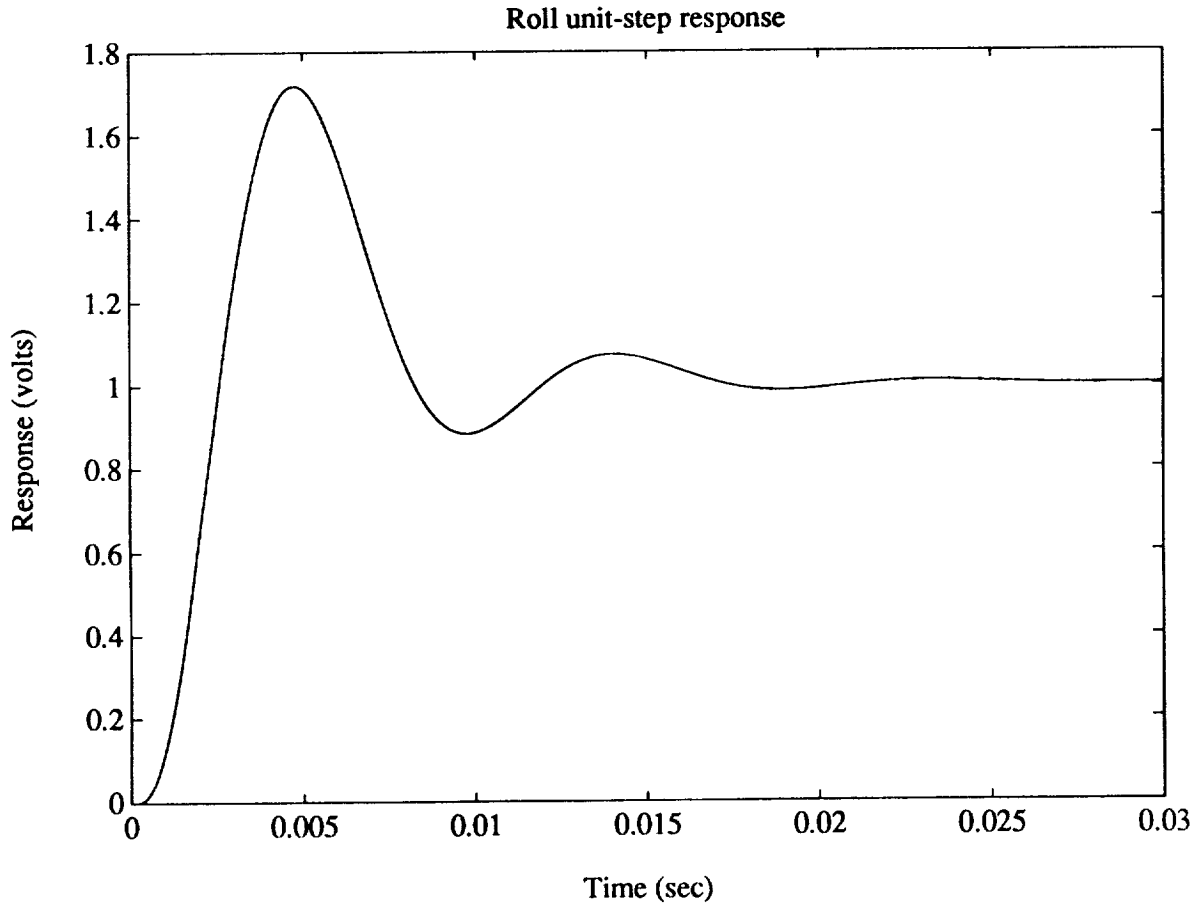

Figure 13: Roll unit-step response predicted by models.

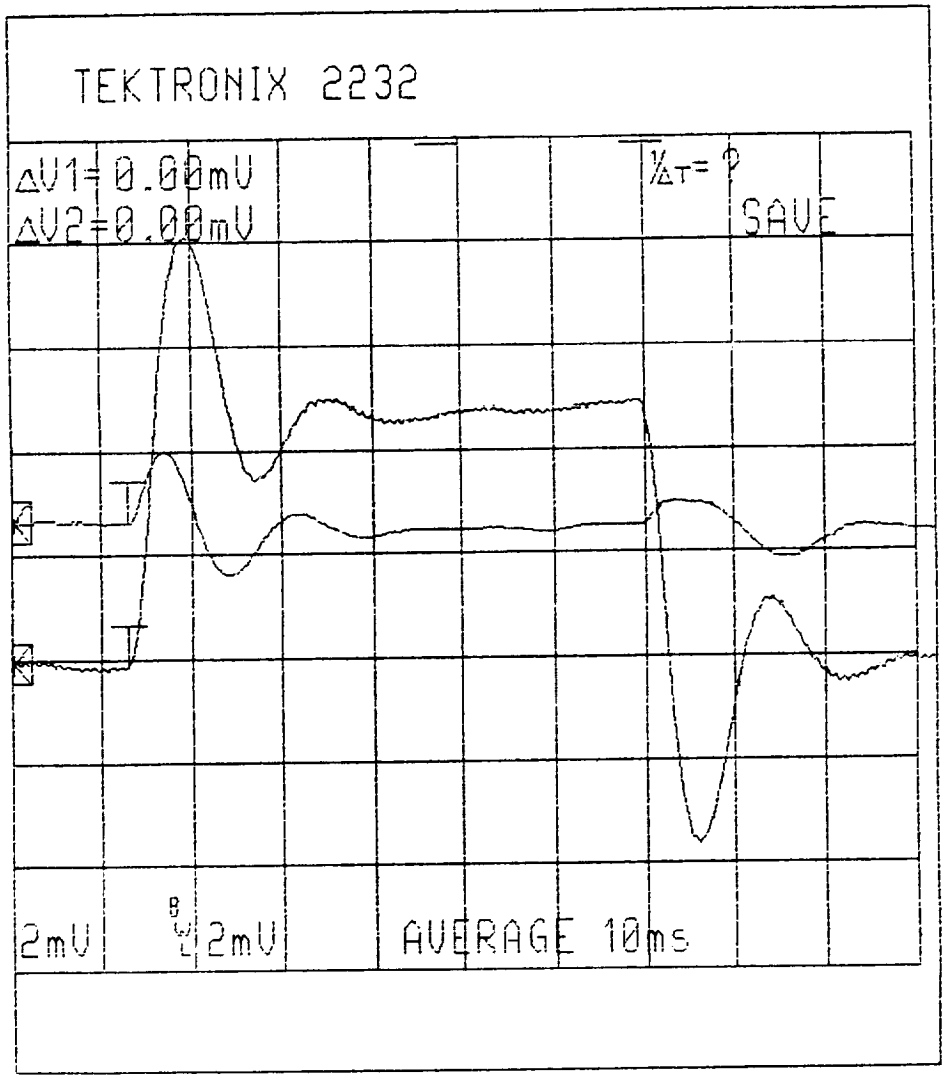

Figure 14: Actual roll step-response $v_{m1}(t)$. Second trace shows undesired cross-coupling response in pitch $v_{m2}(t)$.

Probe #	Crystal Freq. (MHz)	Excitation Freq. (MHz)
1	4.00	1.00
2	5.00	1.25
3	6.00	1.50
4	4.00	1.00
5	5.00	1.25

Table 1: Probe oscillator and excitation frequencies.

the five degrees of freedom which are controlled by the electromagnets. The probes are manufactured by Pioneer Technology, Inc., of Sunnyvale, CA. They operate with an air gap of 0.005". The probes are driven by electronics which produce an output voltage of 5 volts per 0.001" of motion over a travel of ±0.0025". Their specified accuracy is ±0.2% of full scale with a linearity of 0.1% of full scale, and a bandwidth of 10 kHz.

The electronics for all five probes is contained in a single chassis, and consists of a card cage containing individual circuit boards connected to each probe. Each circuit board uses a local quartz crystal oscillator to set the frequency of probe excitation. Unfortunately, only three separate frequencies are used for the five probe boards. This leads to significant beat frequency noise between the probes which are operated at the same nominal frequency. This problem is described in more detail below.

The crystal oscillator is divided down by a factor of 4 to give the probe excitation frequency. The crystal frequencies and excitation frequencies for the five probes are summarized in Table 1. When all five probes are connected, probe pairs #1–#4 and #2–#5 interact with a low frequency beat signal because they are operating on independent but nearly identical frequencies. The beat signal is at about 10 Hz with an amplitude on the order of tenths of a volt. The existence of this beat signal means that the true position stability capabilities of the suspension can not be demonstrated when all five of the probes are in use. They can be demonstrated if some of the probes are disabled; for instance if #4 and #5 are turned off, then the three top electromagnets can be used to stabilize the system in the vertical degrees of freedom, and with low noise contribution from the probes.

This is the approach which has been taken in the current work. The system positioning noise baseline is demonstrated using only the vertical system operating on the first three probes alone. When all five degrees of freedom are controlled, there is significant noise; however, the system step responses can be characterized through averaging on a digital oscilloscope, and the system frequency responses can be measured using a dynamic analyzer since this instrument is inherently narrow-band.

An alternate approach which is clearly more desirable in the long-term is to change the probe operating frequencies so that they run on five independent frequencies. For instance, using crystals at 4.5 and 5.5 MHz to drive probes #4 and #5 will eliminate any low-frequency beat tones. This option will implemented at UNC-Charlotte on the next version of the experimental system, allowing high stability in all five controlled degrees of freedom.

The probe noise-baseline when only the three top probes are connected and are facing fixed targets is shown in Figure 15. The voltages have been low-pass filtered to a 1 kHz bandwidth by a passive network preceding the oscilloscope input. The traces are taken with the oscilloscope in peak detect mode, so that short duration noise pulses are captured. All three probes have output noise voltages on the order of 1 mV p-p. This establishes a noise baseline for the three top electromagnets used alone. An approximately 10 Hz signal can be seen in the trace for probe #2. This is due to cross-coupling with probe #4 even when probe #4 is disconnected from the instrumentation card-cage.

When in suspension, the position stability is currently limited by the probe noise, even when only three degrees of freedom are active. This is demonstrated by the trace shown in Figure 16. The peak-to-peak noise is on the order of that shown with the probes facing a fixed target, i.e., 5 nm. Thus we expect that even higher stability can be demonstrated with probes having lower noise. This is believed to be the highest stability yet demonstrated by a magnetic suspension.

This performance is achieved with the experiment isolated from vibration by an optical table on gas-spring legs. Lightly tapping the optical table or the support brackets with a screwdriver results

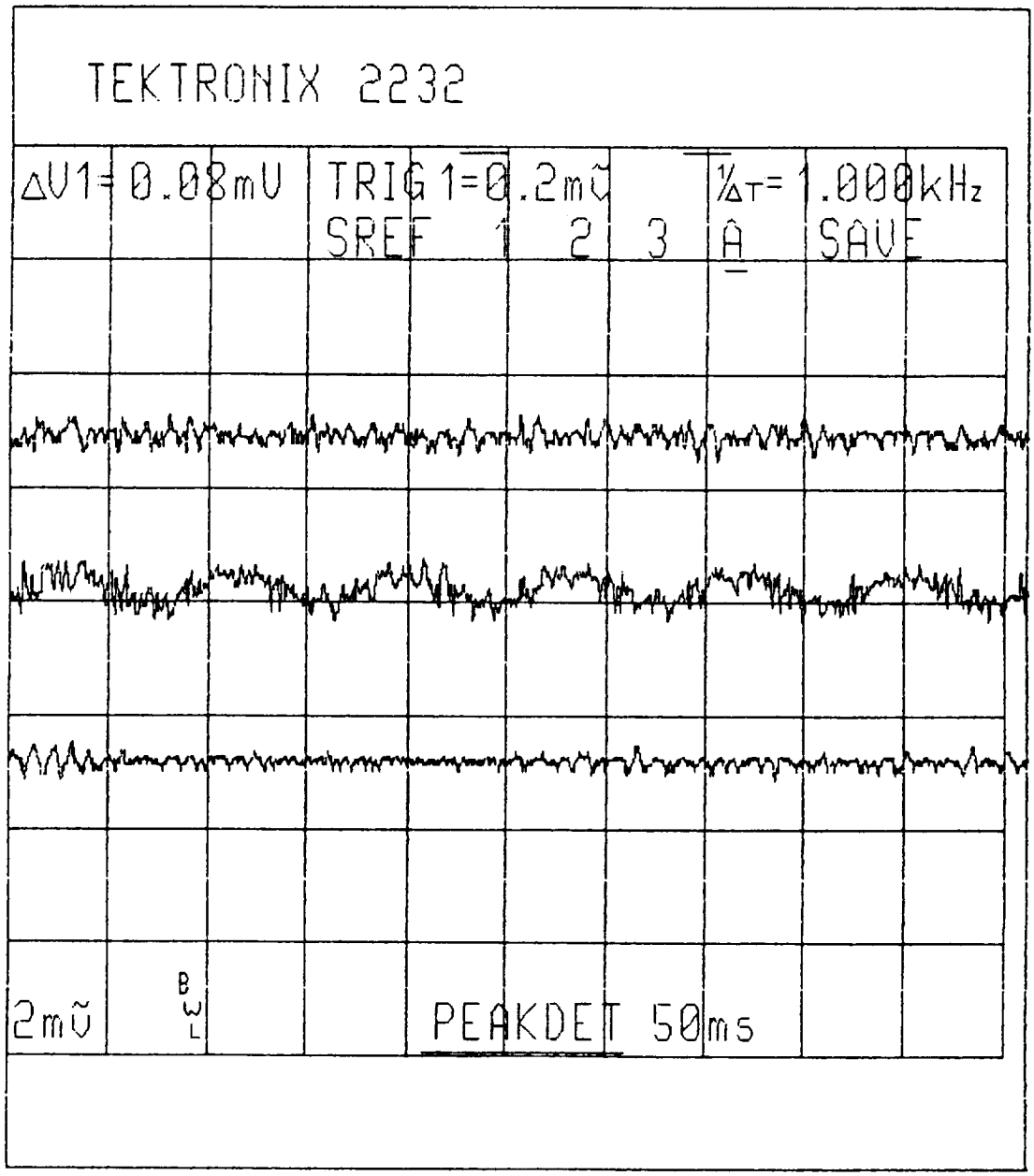

Figure 15: Baseline noise of probes #1, #2, and #3 with probes #4 and #5 disconnected.

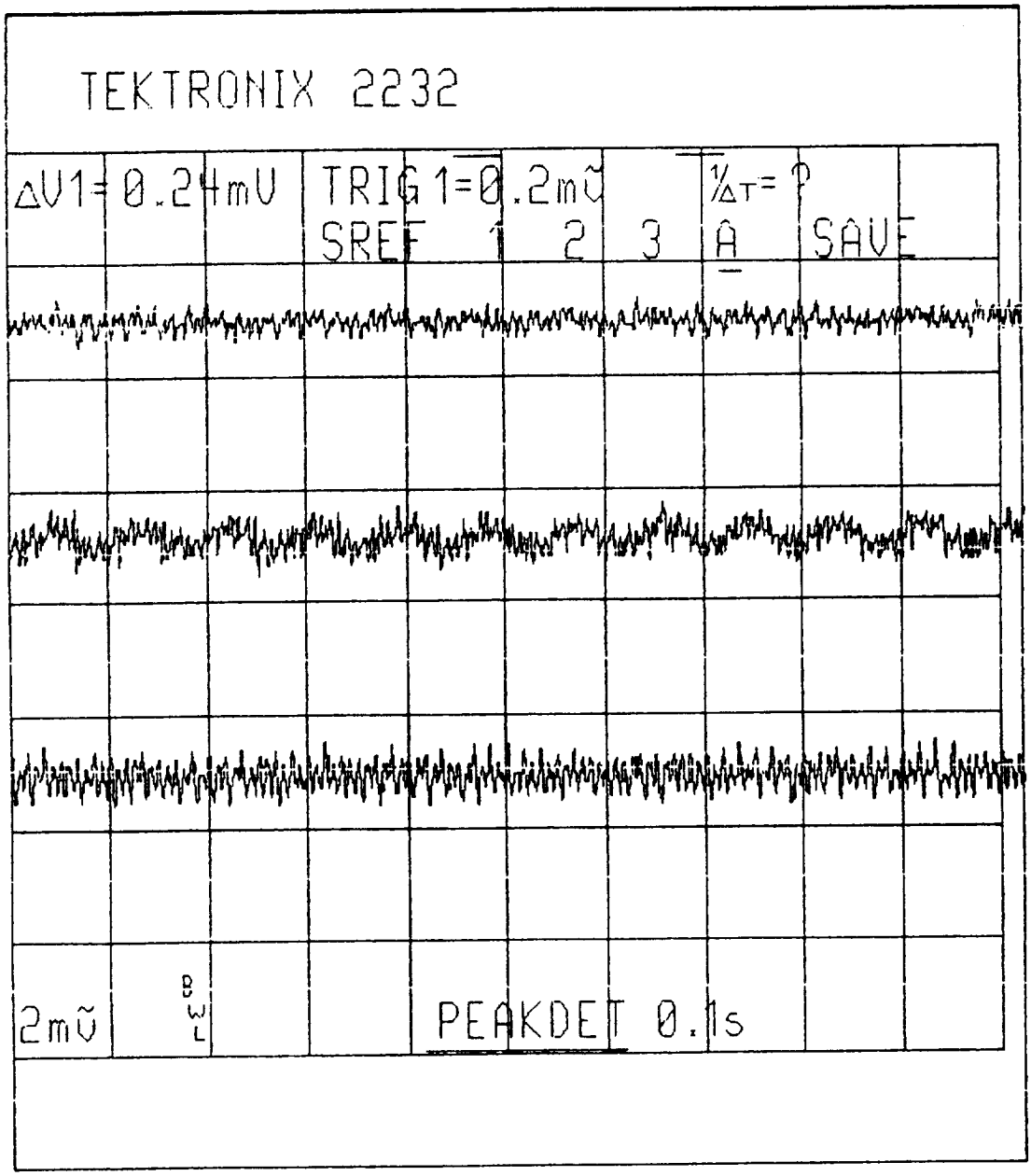

Figure 16: Vertical system suspension stability. Three traces show output voltages of probes #1, #2, and #3 from top to bottom respectively. One millivolt corresponds to approximately 5 nm.

in hundreds of nanometers of motion. Even the relatively stiff support brackets can be deflected by measurable amounts with the application of light finger pressure. These observations help to give a physical feel for the minute motions being measured.

Note that in Figure 16 the low-frequency (10 Hz) signal in the output from probe #2 is attenuated relative to the case where the probe is facing a fixed target. This happens because that component and all low-frequency (relative to loop crossover) noise components in the probe signal are attenuated by the closed position-loop. Thus, under closed-loop conditions the platen is actually moving such that the low-frequency components of the probe noise are nulled. The noise base-line shown in Figure 16 however gives a bound on the magnitude of this effect as less than 5 nm p-p. It is preferable to verify the position stability with an independent measurement such as can be provided by a laser interferometer. This approach will be taken in the current development effort at UNC-Charlotte.

6 Conclusions

A novel linear bearing system has been described which has demonstrated position stability of 5 nm in a low-disturbance environment. This level of stability serves as proof-of-concept for the construction of magnetic bearing systems which address nanometer-resolution motion control. With improved sensors, it is expected that Ångstrom-scale motion control can be achieved, allowing magnetic bearings to be used in stages for scanned probe microscopy with atomic resolution.

7 Acknowledgements

This work forms part of a thesis submitted by the first author to the Department of Electrical Engineering and Computer Science at M.I.T. in partial fulfillment of the requirements for the degree of Doctor of Philosophy [2]. The authors gratefully acknowledge the assistance of Van Pham, Tim Hawkey, Eric Heatzig, Dave Gessel, and Art Rudolf at M.I.T., and Carl Much, Mike Johnson, Pete Rossini, Paul Mitiguy, and Hardy Prince at M.I.T. Lincoln Laboratory. This work was sponsored by the Department of the Air Force, and performed at the M.I.T. Lincoln Laboratory.

8 References

[1] Slocum, A.H., and Eisenhaure, D.B., "Design Considerations for Ultra-Precision Magnetic Bearing Supported Slides," NASA Magnetic Suspension Technology Conference, Hampton, Va. Feb. 2-4, 1988.

[2] Trumper, D.L., "Magnetic Suspension Techniques for Precision Motion Control," Ph.D. Thesis, Dept. of Elec. Eng. and Comp. Sci., M.I.T., Camb., Mass., Sept., 1990.

[3] Trumper, D.L., "Nonlinear Compensation Techniques for Magnetic Suspension Systems," NASA Workshop on Aerospace Applications of Magnetic Suspension Technology, Hampton, VA, Sept. 25-27, 1990.

9 Appendix

The numerical values of the vertical suspension matrices are shown below.

```
Av =

  Columns 1 through 6

 -6.6667e+03  -8.3333e+06            0            0            0            0
  1.0000e+00            0            0            0            0            0
           0            0  -6.6667e+03  -8.3333e+06            0            0
           0            0   1.0000e+00            0            0            0
           0            0            0            0  -6.6667e+03  -8.3333e+06
```

```
         0         0         0         0    1.0000e+00         0
         0         0         0         0             0         0
         0         0         0         0             0         0
         0         0         0         0             0         0
         0         0         0    1.9399e+08         0   -1.9399e+08
         0   -4.0981e+08         0    1.9837e+08         0    1.9837e+08
         0    5.6048e+07         0    2.7130e+07         0    2.7130e+07

  Columns 7 through 12

         0         0         0         0         0         0
         0         0         0         0         0         0
         0         0         0         0         0         0
         0         0         0         0         0         0
         0         0         0         0         0         0
         0         0         0         0         0         0
         0         0         0    1.0000e+00         0         0
         0         0         0         0    1.0000e+00         0
         0         0         0         0         0    1.0000e+00
 1.1936e+04         0         0         0         0         0
         0   3.1654e+04   1.9098e+04         0         0         0
         0   2.4051e+02   4.7015e+04         0         0         0

Bv =

     1     0     0
     0     0     0
     0     1     0
     0     0     0
     0     0     1
     0     0     0
     0     0     0
     0     0     0
     0     0     0
     0     0     0
     0     0     0
     0     0     0

Cv =

     0     0     0     0     0     0     1     0     0     0     0     0
     0     0     0     0     0     0     0     1     0     0     0     0
     0     0     0     0     0     0     0     0     1     0     0     0

Dv =

     0     0     0
     0     0     0
     0     0     0
```